

# Predictions of the optimized friction stir spot welding process parameters for joining AA2024 aluminum alloy using RSM

R. Karthikeyan · V. Balasubramanian

Received: 8 November 2009 / Accepted: 8 March 2010 / Published online: 1 April 2010  
© Springer-Verlag London Limited 2010

**Abstract** The friction stir spot welding process (FSSW) is a variant of the linear friction stir welding process in which the material is being welded without bulk melting. The FSSW parameters such as tool rotational speed, plunge rate, plunge depth, and dwell time play a major role in determining the strength of the joints. A central composite rotatable design with four factors and five levels was chosen to minimize the number of experimental conditions. An empirical relationship was established to predict the tensile shear fracture load of friction stir spot-welded AA2024 aluminum alloy by incorporating independently controllable FSSW process parameters. Response surface methodology (RSM) was applied to optimize the FSSW parameters to attain maximum lap shear strength of the spot weld.

**Keywords** Friction stir spot welding · Aluminum alloy · Response surface methodology · Optimization

## Nomenclature

FSW	Friction stir welding
FSSW	Friction stir spot welding
ERSW	Electrical resistance spot welding
$N$	Tool rotational speed, rpm
$R$	Plunge rate, mm/min
$D$	Plunge depth, mm

$T$	Dwell time, s
TSFL	Tensile shear fracture load, kN
RSM	Response surface methodology

## 1 Introduction

To meet the challenges for future automotive regarding emissions, safety, and sustainability, aluminum is the most prominent candidate to be increasingly used, but welding of aluminum with the conventional electrical resistance spot welding (ERSW) is highly difficult, as the surfaces to be joined must be kept cleaned and free from surface oxides. Moreover, electrode wear limits electrode life to 1,000 spots whereas 10,000 spots when welding steel [1]. Friction stir spot welding (FSSW) is an ideal competent process for aluminum welding than ERSW. FSSW is a derivative process of friction stir welding process. FSSW is a single spot joining process, in which a solid-state joining is made between adjacent materials at overlap configuration. This process also eradicates the problems associated with commonly used other single spot joining processes such as mechanical riveting, clinching, and toggle lock [2–5].

Pan et al. [6] studied the effect of tool penetration depth at a constant tool rotational speed and reported different failure modes such as interfacial separation at shallow insertion depths, nugget pullout at highest strength, and perimeter failure at deepest insertion. Arul et al. [7] investigated the microstructures and failure mechanisms of FSSW AA5754 aluminum alloy and reported that the failure mechanism was necking and shearing. Mitlin et al. [8] reported that the tool pin penetration depth had a strong effect on the failure mode

R. Karthikeyan · V. Balasubramanian (✉)  
Department of Manufacturing Engineering, Annamalai University,  
Annamalainagar,  
608 002 Chidambaram, Tamil Nadu, India  
e-mail: visvabalu@yahoo.com

R. Karthikeyan  
e-mail: rkyen22@yahoo.com

of the joints and a lesser effect on the joint shear strength. Yasunari et al. [9] studied the effect of various FSSW parameters on bonding strength and reported that plunge depth was an important variable affecting bonding area and strength. Wang et al. [10] reported the fatigue lives of friction stir spot welds of aluminum alloys. The effect of pin geometry on the hook formation was analyzed by Badarinarayanan et al. [11].

It is well known that the input welding parameters play a major role in determining the weld quality. As the process facts have not been disclosed so far, the selection of input parameters to join aluminum alloy is very difficult. While welding of aluminum alloy with conventional process is a problem, achieving the optimized weld quality with a new process such as FSSW is a huge problem. Hence, the problem of getting optimized weld parameters to attain maximum lap shear tensile strength is attempted in this investigation.

## 2 Experimental work

In this investigation, the rolled sheet of 2.7-mm thickness, AA2024-T3 aluminum alloy, was used to fabricate the joints. The sheet was cut to required size by power hacksaw cutting and followed by grinding to remove the burr. The chemical composition and mechanical properties of the base metal are presented in Tables 1 and 2, respectively. Lap joint configuration was used to fabricate the spot welds where the rolling direction of material was kept parallel to the loading directions, and the joint was initially obtained by securing the plates in position using mechanical clamps. A nonconsumable tool made of high-carbon steel was used to fabricate the joints. The tool with a flat cylindrical shoulder diameter of 16.2 mm and a 0.8-mm pitch metric, left hand threaded pin of 5.4-mm diameter, was used. An indigenously designed and developed computer numerical controlled friction stir spot welding machine (4,000 rpm, 22 kW, 6 t) was used. The welding experiments were carried out under displacement control mode. Lap shear tensile specimens were prepared as per the dimensions shown in Fig. 1.

From the literature, the predominant factors having significant influence on the performance of FSSW joints

**Table 1** Chemical composition (weight percent) of aluminum alloy AA2024-T3

Cu	Mg	Mn	Fe	Si	Cr	Zn	Ti	Al
4.8	1.80	0.90	0.50	0.50	0.10	0.25	0.15	Bal

**Table 2** Mechanical properties of aluminum alloy AA2024-T3

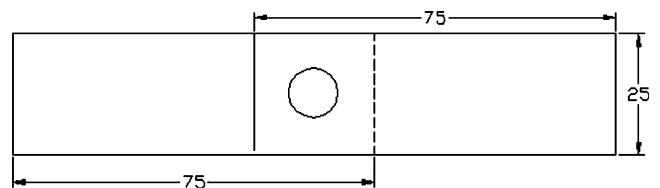
Tensile yield strength (MPa)	Ultimate tensile strength (MPa)	Shear strength (MPa)	Elongation in 50-mm gauge length (%)	Hardness at 0.05kg of load (Hv)
345	483	283	18	137

were identified. They are (a) tool rotational speed, (b) plunge rate, (c) plunge depth, and (d) dwell time. A large number of trial experiments were conducted to determine the working range of the above factors by varying one of the process parameters and keeping the rest of them at constant value. The working range was fixed in such a way by considering the absence of visible defects, the existence of weld between the sheets, and avoiding markedly low values of tensile shear fracture load (TSFL). The chosen welding parameters and their levels are presented in Table 3.

As the range of individual factor was wide, a central composite rotatable four-factor, five-level factorial design matrix was selected. The experimental design matrix (Table 4) consisting 30 sets of coded condition and comprising a full replication four-factor factorial design of 16 points, 8 star points, and 6 center points was used. The upper and lower limits of the parameters were coded as +2 and -2, respectively. The coded values for intermediate levels can be calculated from the relationship.

$$X_i = 2[2X - (X_{\max} + X_{\min})]/[X_{\max} - X_{\min}] \quad (1)$$

where  $X_i$  is the required coded value of a variable  $X$  and  $X$  is any value of the variable from  $X_{\min}$  to  $X_{\max}$ . The spot welds were made as per the conditions dictated by the design matrix at random order so as to avoid the noise creeping output response. At each condition, three specimens were fabricated. Some of the fabricated FSSW lap joints are displayed in Fig. 2. Lap shear test was carried out in 100-kN electromechanically controlled Universal Testing Machine (FIE-Bluestar, India; model UNITEK-94100). The specimen was loaded at the rate of 1.5 kN/min as per ASTM specifications until the faying surfaces of specimen



**Fig. 1** Configuration of a lap shear test specimen

**Table 3** Important factors and their levels

No.	Factor	Unit	Notation	Levels				
				-2	-1	0	1	2
1	Tool rotational speed	rpm	<i>N</i>	600	800	1,000	1,200	1,400
2	Plunge rate	mm/min	<i>R</i>	4	8	12	16	20
3	Plunge depth	mm	<i>D</i>	4.4	4.6	4.8	5.0	5.2
4	Dwell time	s	<i>T</i>	3	4	5	6	7

were sheared off, and the values were recorded. Average of three tensile lap shear-tested specimen values was used for optimization. Four different types of failure modes were observed after tensile testing. They are eyelet, interfacial,

partially curved interfacial, and nugget pullout. Table 5 presents the observations from fractured samples (top and bottom views of upper sheet and top view of lower sheet) of friction stir spot welds.

**Table 4** Design matrix and experimental results

Expt. no.	Coded value				Original value				Tensile shear fracture load (with SD; kN)
	<i>N</i>	<i>R</i>	<i>D</i>	<i>T</i>	<i>N</i>	<i>R</i>	<i>D</i>	<i>T</i>	
1	-1	-1	-1	-1	800	8	4.6	4	6.15 (0.15)
2	+1	-1	-1	-1	1,200	8	4.6	4	6.56 (0.14)
3	-1	+1	-1	-1	800	16	4.6	4	6.70 (0.11)
4	+1	+1	-1	-1	1,200	16	4.6	4	7.51 (0.16)
5	-1	-1	+1	-1	800	8	5.0	4	7.08 (0.11)
6	+1	-1	+1	-1	1,200	8	5.0	4	7.20 (0.09)
7	-1	+1	+1	-1	800	16	5.0	4	7.43 (0.07)
8	+1	+1	+1	-1	1,200	16	5.0	4	7.98 (0.19)
9	-1	-1	-1	+1	800	8	4.6	6	6.76 (0.14)
10	+1	-1	-1	+1	1,200	8	4.6	6	7.24 (0.15)
11	-1	+1	-1	+1	800	16	4.6	6	7.27 (0.13)
12	+1	+1	-1	+1	1,200	16	4.6	6	8.03 (0.20)
13	-1	-1	+1	+1	800	8	5.0	6	7.60 (0.13)
14	+1	-1	+1	+1	1,200	8	5.0	6	7.39 (0.12)
15	-1	+1	+1	+1	800	16	5.0	6	8.07 (0.07)
16	+1	+1	+1	+1	1,200	16	5.0	6	8.16 (0.17)
17	-2	0	0	0	600	12	4.8	5	5.95 (0.13)
18	+2	0	0	0	1,400	12	4.8	5	6.80 (0.15)
19	0	-2	0	0	1,000	4	4.8	5	6.77 (0.10)
20	0	+2	0	0	1,000	20	4.8	5	8.20 (0.11)
21	0	0	-2	0	1,000	12	4.4	5	8.15 (0.20)
22	0	0	+2	0	1,000	12	5.2	5	9.19 (0.17)
23	0	0	0	-2	1,000	12	4.8	3	5.71 (0.12)
24	0	0	0	+2	1,000	12	4.8	7	6.65 (0.06)
25	0	0	0	0	1,000	12	4.8	5	9.47 (0.18)
26	0	0	0	0	1,000	12	4.8	5	8.87 (0.15)
27	0	0	0	0	1,000	12	4.8	5	8.92 (0.22)
28	0	0	0	0	1,000	12	4.8	5	8.81 (0.13)
29	0	0	0	0	1,000	12	4.8	5	9.01 (0.22)
30	0	0	0	0	1,000	12	4.8	5	9.20 (0.14)

### 3 Developing an empirical relationship

TSFL of friction stir spot-welded AA2024 aluminum alloy is a function of the welding parameters such as tool rotational speed (*N*), plunge rate (*R*), plunge depth (*D*), and dwell time (*T*), and it can be expressed as

$$TSFL = f(N, R, D, T). \tag{2}$$

The second-order polynomial (regression) equation used to represent the response surface *Y* is given by

$$Y = b_0 + \sum b_i x_i + \sum b_{ii} x_i^2 + \sum b_{ij} x_i x_j, \tag{3}$$

and for four factors, the selected polynomial could be expressed as

$$TSFL = b_0 + b_1(N) + b_2(R) + b_3(D) + b_4(T) + b_{12}(NR) + b_{13}(ND) + b_{14}(NT) + b_{23}(RD) + b_{24}(RT) + b_{34}(DT) + b_{11}(N^2) + b_{22}(R^2) + b_{33}(D^2) + b_{44}(T^2) \tag{4}$$

where *b*<sub>0</sub> is the average of the responses and *b*<sub>1</sub>, *b*<sub>2</sub>, *b*<sub>3</sub>, ..., *b*<sub>44</sub> are regression coefficients[12] that depend on respective linear, interaction, and squared terms of factors. The value of the coefficient was calculated using Design Expert Software. The significance of each coefficient was determined by Student's *t* test and *p* values, which are listed in Table 6. Values of “Prob>*F*” less than 0.0500 indicate that model terms are significant. In this case, *N*, *R*, *D*, *T*, *ND*, *N*<sup>2</sup>, *R*<sup>2</sup>, and *T*<sup>2</sup> are significant model terms. Values greater than 0.10 indicate that model terms are not significant. The results of multiple linear regression coefficients for the second-order response surface model are given in Table 7. The final

**Fig. 2** A photograph of AA2024 friction stir spot-welded lap shear specimens



empirical relationship was constructed using only these coefficients, and the developed final empirical relationship is given below:

$$\begin{aligned} \text{TSFL} = \{ & 9.046 + 0.196(N) + 0.334(R) + 0.282(D) \quad (5) \\ & + 0.241(T) - 0.119(\text{ND}) - 0.644(N^2) \\ & - 0.366(R^2) - 0.692(T^2) \} \text{kN} \end{aligned}$$

Analysis of variance (ANOVA) technique was used to check the adequacy of the developed empirical relationship. In this investigation, the desired level of confidence was considered to be 95%. The relationship may be considered to be adequate provided that (a) the calculated value of the  $F$  ratio of the model developed should not exceed the standard tabulated value of  $F$  ratio and (b) the calculated value of the  $R$  ratio of the developed relationship should exceed the standard tabulated value of  $R$  ratio for a desired level of confidence. It is found that the model is adequate. The model  $F$  value of 67.35 implies that the model is significant. There is only a 0.01% chance that a model  $F$  value this large could occur due to noise. The lack of fit  $F$  value of 0.28 implies that the lack of fit is insignificant. There is only a 0.04% chance that a lack of fit  $F$  value this large could occur due to noise. Each predicted value matches its experimental value well as shown in Fig. 3.

The Fisher's  $F$  test with a very low probability value ( $P_{\text{model}} > F = 0.0001$ ) demonstrates a very high signifi-

cance for the regression model. The goodness of fit of the model was checked by the determination coefficient ( $R^2$ ). The coefficient of determination ( $R^2$ ) was calculated to be 0.9843 for response. This implies that 98.4% of experimental data confirms the compatibility with the data predicted by the model, and the model does not explain only 1.57% of the total variations. The  $R^2$  value is always between 0 and 1, and its value indicates aptness of the model. For a good statistical model,  $R^2$  value should be close to 1.0. The adjusted  $R^2$  value reconstructs the expression with the significant terms. The value of the adjusted determination coefficient ( $\text{Adj } R^2 = 0.9697$ ) is also high to advocate for a high significance of the model. The  $\text{Pred } R^2$  is 0.9528 that implies that the model could explain 95% of the variability in predicting new observations. This is in reasonable agreement with the  $\text{Adj } R^2$  of 0.9697. The value of coefficient of variation is also low as 2.35 indicates that the deviations between experimental and predicted values are low. Adeq precision measures the signal to noise ratio. A ratio greater than 4 is desirable. In this investigation, the ratio is 27.859, which indicates an adequate signal. This model can be used to navigate the design space.

#### 4 Optimizing the welding parameters

The response surface methodology (RSM) was used to optimize the parameters in this study. RSM is a collection of mathematical and statistical techniques that are useful for



**Table 5** Observations from fractured samples




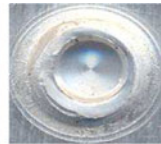











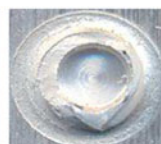




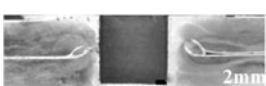



























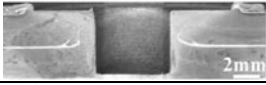


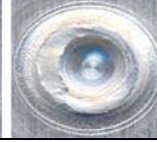















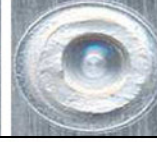















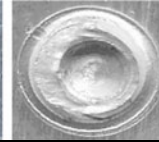
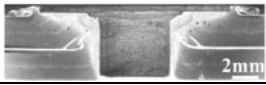



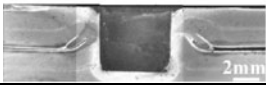



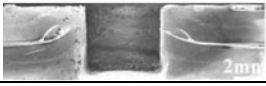







No	Parameters	Cross sectional Macrostructure	Top view of top sheet	Bottom view of top sheet	Top view of bottom sheet	Observations
1	$N = 800$ $R = 8$ $D = 4.6$ $T = 4$					TSFL = 6.15 kN Fracture: eyelet Flash level: excess Material mixing: less
2	$N = 1200$ $R = 8$ $D = 4.6$ $T = 4$					TSFL = 6.56 kN Fracture: eyelet Flash level: normal Material mixing: less
3	$N = 800$ $R = 16$ $D = 4.6$ $T = 4$					TSFL = 6.7 kN Fracture: eyelet Flash level: normal Material mixing: less
4	$N = 1200$ $R = 16$ $D = 4.6$ $T = 4$					TSFL = 7.51 kN Fracture: partially curved interfacial Flash level: normal Material mixing: good
5	$N = 800$ $R = 8$ $D = 5.0$ $T = 4$					TSFL = 7.08 kN Fracture: eyelet Flash level: excess Material mixing: good
6	$N = 1200$ $R = 8$ $D = 5.0$ $T = 4$					TSFL = 7.2 kN Fracture: eyelet Flash level: excess Material mixing: good
7	$N = 800$ $R = 16$ $D = 5.0$ $T = 4$					TSFL = 7.43 kN Fracture: partially curved interfacial Flash level: normal Material mixing: good
8	$N = 1200$ $R = 16$ $D = 5.0$ $T = 4$					TSFL = 7.98 kN Fracture: partially curved interfacial Flash level: less Material mixing: good
9	$N = 800$ $R = 8$ $D = 4.6$ $T = 6$					TSFL = 6.76 kN Fracture: eyelet Flash level: normal Material mixing: less
10	$N = 1200$ $R = 8$ $D = 4.6$ $T = 6$					TSFL = 7.24kN Fracture: eyelet Flash level: excess Material mixing: good

Table 5 (continued)

11	$N = 800$ $R = 16$ $D = 4.6$ $T = 6$					TSFL = 7.27 kN Fracture: partially curved interfacial Flash level: normal Material mixing: good
12	$N = 1200$ $R = 16$ $D = 4.6$ $T = 6$					TSFL = 8.03 kN Fracture: partially curved interfacial Flash level: less Material mixing: very good
13	$N = 800$ $R = 8$ $D = 5.0$ $T = 6$					TSFL = 7.6 kN Fracture: partially curved interfacial Flash level: normal Material mixing: good
14	$N = 1200$ $R = 8$ $D = 5.0$ $T = 6$					TSFL = 7.39 kN Fracture: partially curved interfacial Flash level: less Material mixing: good
15	$N = 800$ $R = 16$ $D = 5.0$ $T = 6$					TSFL = 8.07 kN Fracture: partially curved interfacial Flash level: normal Material mixing: very good
16	$N = 1200$ $R = 16$ $D = 5.0$ $T = 6$					TSFL = 8.16 kN Fracture: partially curved interfacial Flash level: normal Material mixing: very good
17	$N = 600$ $R = 12$ $D = 4.8$ $T = 5$					TSFL = 5.95 kN Fracture: interfacial Flash level: excess Material mixing: less
18	$N = 1400$ $R = 12$ $D = 4.8$ $T = 5$					TSFL = 6.8 kN Fracture: eyelet Flash level: excess Material mixing: less
19	$N = 1000$ $R = 4$ $D = 4.8$ $T = 5$					TSFL = 6.77 kN Fracture: eyelet Flash level: excess Material mixing: less
20	$N = 1000$ $R = 20$ $D = 4.8$ $T = 5$					TSFL = 8.2 kN Fracture: partially curved interfacial Flash level: normal Material mixing: very good



**Table 5** (continued)

21	$N = 1000$ $R = 12$ $D = 4.4$ $T = 5$					TSFL = 8.15 kN Fracture: partially curved interfacial Flash level: less Material mixing: very good
22	$N = 1000$ $R = 12$ $D = 5.2$ $T = 5$					TSFL = 9.19 kN Fracture: nugget pull out Flash level: normal Material mixing: very good
23	$N = 1000$ $R = 12$ $D = 4.8$ $T = 3$					TSFL = 5.71 kN Fracture: Interfacial Flash level: excess Material mixing: less
24	$N = 1000$ $R = 12$ $D = 4.8$ $T = 7$					TSFL = 6.65 kN Fracture: eyelet Flash level: excess Material mixing: less
25	$N = 1000$ $R = 12$ $D = 4.8$ $T = 5$					TSFL = 9.47 kN Fracture: nugget pull out Flash level: less Material mixing: very good

**Table 6** ANOVA test results

Source	Sum of squares	<i>df</i>	Mean square	<i>F</i> value	<i>p</i> value Prob> <i>F</i>
Model	30.38808	14	2.170577	67.34532	<0.0001 <sup>a</sup>
<i>N-N</i> <sup>a</sup>	0.924337	1	0.924337	28.67892	<0.0001
<i>R-R</i> <sup>a</sup>	2.686704	1	2.686704	83.35892	<0.0001
<i>D-D</i> <sup>a</sup>	1.909704	1	1.909704	59.25136	<0.0001
<i>T-T</i> <sup>a</sup>	1.396838	1	1.396838	43.33892	<0.0001
<i>NR</i>	0.124256	1	0.124256	3.855231	0.0684
<i>ND</i> <sup>a</sup>	0.228006	1	0.228006	7.074226	0.0178
<i>NT</i>	0.037056	1	0.037056	1.149724	0.3006
<i>RD</i>	0.011556	1	0.011556	0.35855	0.5582
<i>RT</i>	0.000506	1	0.000506	0.015707	0.9019
<i>DT</i>	0.045156	1	0.045156	1.401039	0.2550
<i>N</i> <sup>2a</sup>	11.37782	1	11.37782	353.0136	<0.0001
<i>R</i> <sup>2a</sup>	3.685524	1	3.685524	114.3488	<0.0001
<i>D</i> <sup>2</sup>	0.135603	1	0.135603	4.207271	0.0581
<i>T</i> <sup>2a</sup>	13.16542	1	13.16542	408.4763	<0.0001
Residual	0.483458	15	0.032231		
lack of fit	0.176125	10	0.017613	0.286537	0.9562 <sup>b</sup>
Pure error	0.307333	5	0.061467		
Cor total	30.87154	29			

SD=0.179529, mean=7.627667, CV%=2.353652, PRESS=1.45704,  $R^2 = 0.98434$ , Adj  $R^2 = 0.969723$ , Pred  $R^2 = 0.952803$ , Adeq precision=27.85962

*df* degrees of freedom, *CV* coefficient of variation, *F* Fisher's ratio, *p* probability

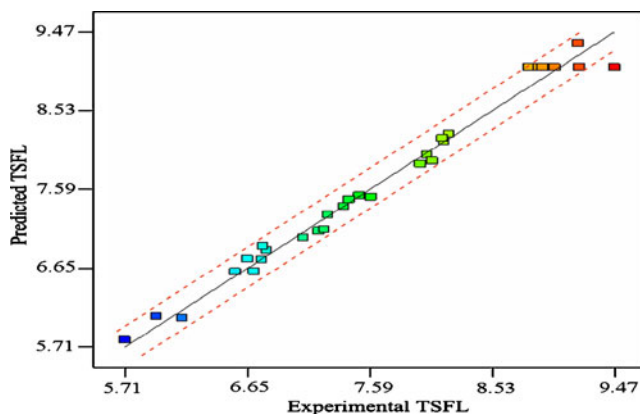
<sup>a</sup> Significant

<sup>b</sup> Not significant

**Table 7** Estimated regression coefficients

Factor	Estimated coefficient
Intercept	9.046667
<i>N-N</i>	0.19625
<i>R-R</i>	0.334583
<i>D-D</i>	0.282083
<i>T-T</i>	0.24125
<i>NR</i>	0.088125
<i>ND</i>	-0.11938
<i>NT</i>	-0.04812
<i>RD</i>	-0.02687
<i>RT</i>	-0.00562
<i>DT</i>	-0.05312
<i>N<sup>2</sup></i>	-0.64406
<i>R<sup>2</sup></i>	-0.36656
<i>D<sup>2</sup></i>	-0.07031
<i>T<sup>2</sup></i>	-0.69281

designing a set of experiments, developing a mathematical model, analyzing for the optimum combination of input parameters, and expressing the values graphically [13, 14]. To obtain the influencing nature and optimized condition of the process on TSFL, the surface plots and contour plots which are the indications of possible independence of factors have been developed for the proposed empirical relation by considering two parameters in the middle level and two parameters in the *x*- and *y*-axes as shown in Fig. 4. These response contours can help in the prediction of the response (TSFL) for any zone of the experimental domain [15]. The apex of the response plot shows the maximum achievable TSFL. A contour plot is produced to display the region of the optimal factor settings visually. For second-order responses, such a plot can be more complex compared to the simple series of parallel lines that can occur with first-order models. Once

**Fig. 3** Correlation graph

**Fig. 4** Response graphs and contour plots. **a, b** Interaction effect of tool rotational speed and plunge rate. **c, d** Interaction effect of tool rotational speed and plunge depth. **e, f** Interaction effect of tool rotational speed and dwell time. **g, h** Interaction effect of plunge rate and plunge depth. **i, j** Interaction effect of plunge rate and dwell time. **k, l** Interaction effect of plunge depth and dwell time

the stationary point is found, it is usually necessary to characterize the response surface in the immediate vicinity of the point. Characterization involves identifying whether the stationary point is a minimum response or maximum response or a saddle point. To classify this, it is most straightforward to examine it through a contour plot. Contour plots play a very important role in the study of a response surface. It is clear from Fig. 4 that the TSFL increases with the increase of tool rotational speed, plunge rate, and dwell time to a certain value and then decreases. It is also observed that the initial increase of plunge depth increases the TSFL to a certain value and further increase of plunge depth makes the TSFL remain constant.

By analyzing the response surfaces and contour plots (Fig. 4), the maximum achievable TSFL value is found to be 9.39 kN. The corresponding parameters that yielded this maximum value are tool rotational speed of 1,000 rpm, plunge rate of 13.56 mm/min, plunge depth of 5.178 mm, and dwell time of 5.1 s.

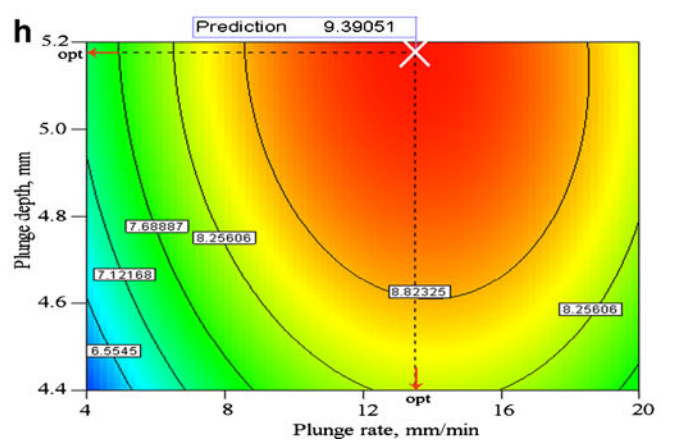
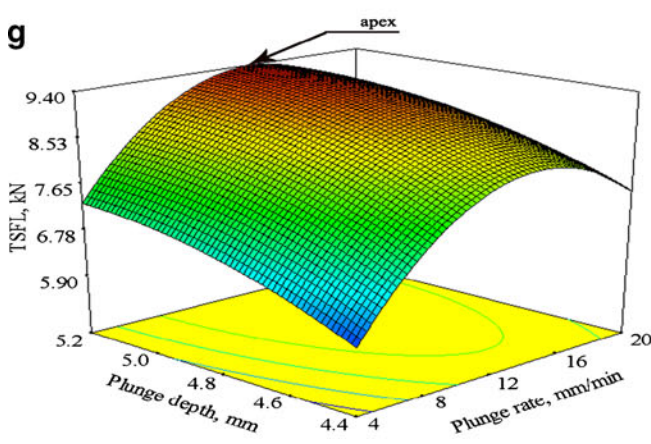
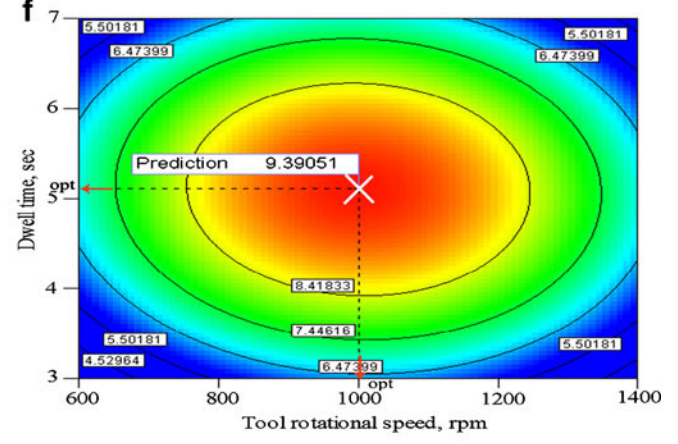
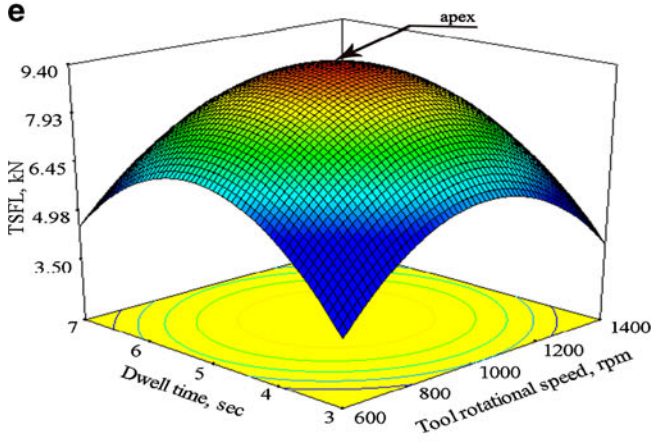
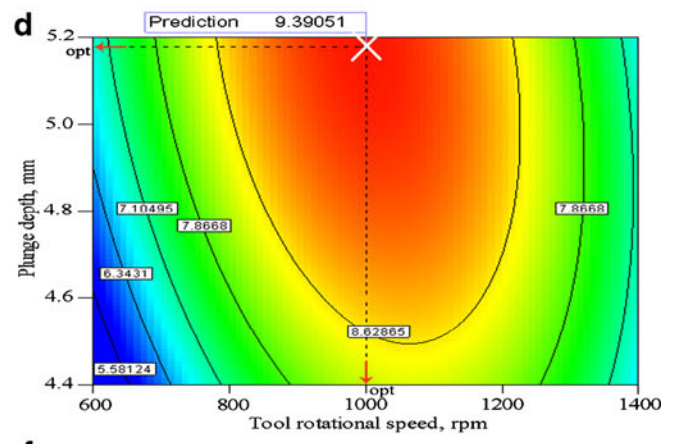
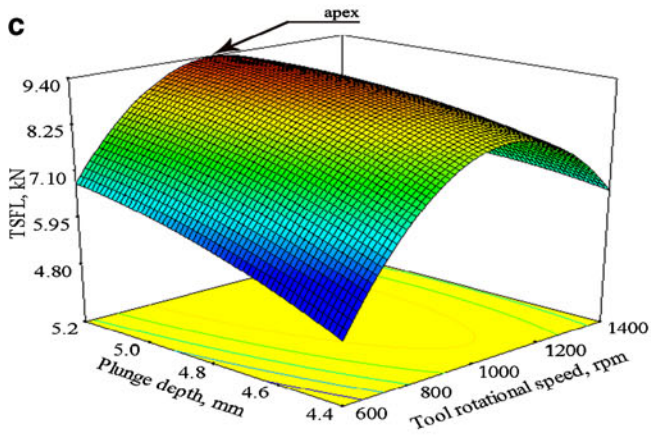
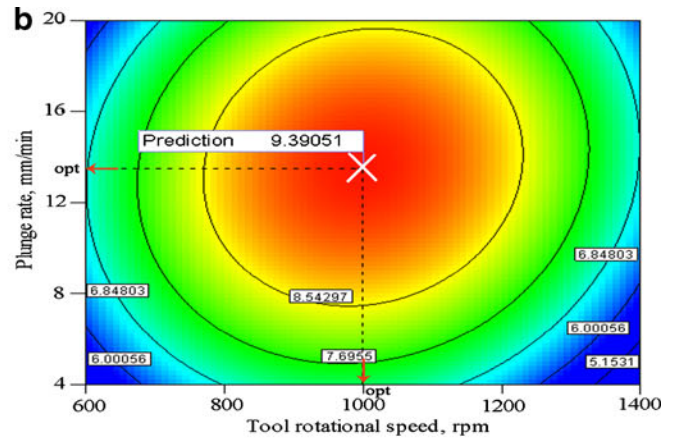
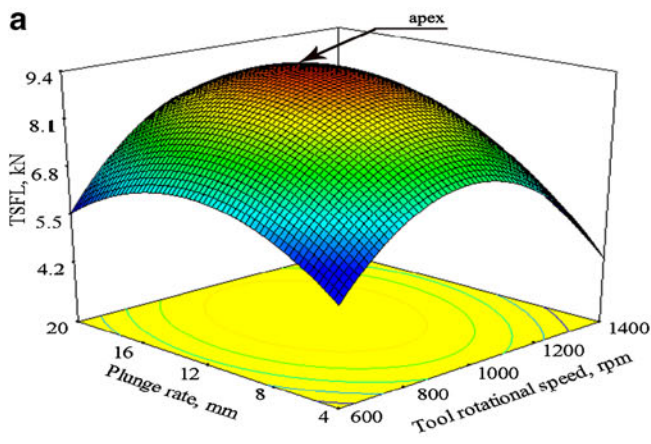
Contributions made by the process parameters on tensile shear failure load can be ranked [16, 17] from their respective *F* ratio value which was seen in Table 6, provided the degrees of freedom are same for all the input parameters. The higher *F* ratio value implies that the respective term is more significant and vice versa.

From the *F* ratio values, it can be concluded that plunge rate is contributing more on tensile shear failure load, and it is followed by plunge depth, dwell time, and tool rotational speed for the range considered in this investigation.

## 5 Conclusions

1. An empirical relationship was developed to predict the tensile shear fracture load of friction stir spot-welded AA2024-T3 aluminum alloy joints incorporating welding parameters at 95% confidence level.
2. A maximum tensile shear fracture load of 9.39 kN could be attained under the welding conditions of 1,000 rpm of tool rotational speed, 13.56 mm/min of plunge rate, 5.178 mm of plunge depth, and 5.1 s of dwell time.
3. Of the four process parameters investigated, the plunge rate was found to have greater influence on tensile shear fracture load followed by plunge depth, dwell time, and tool rotational speed.





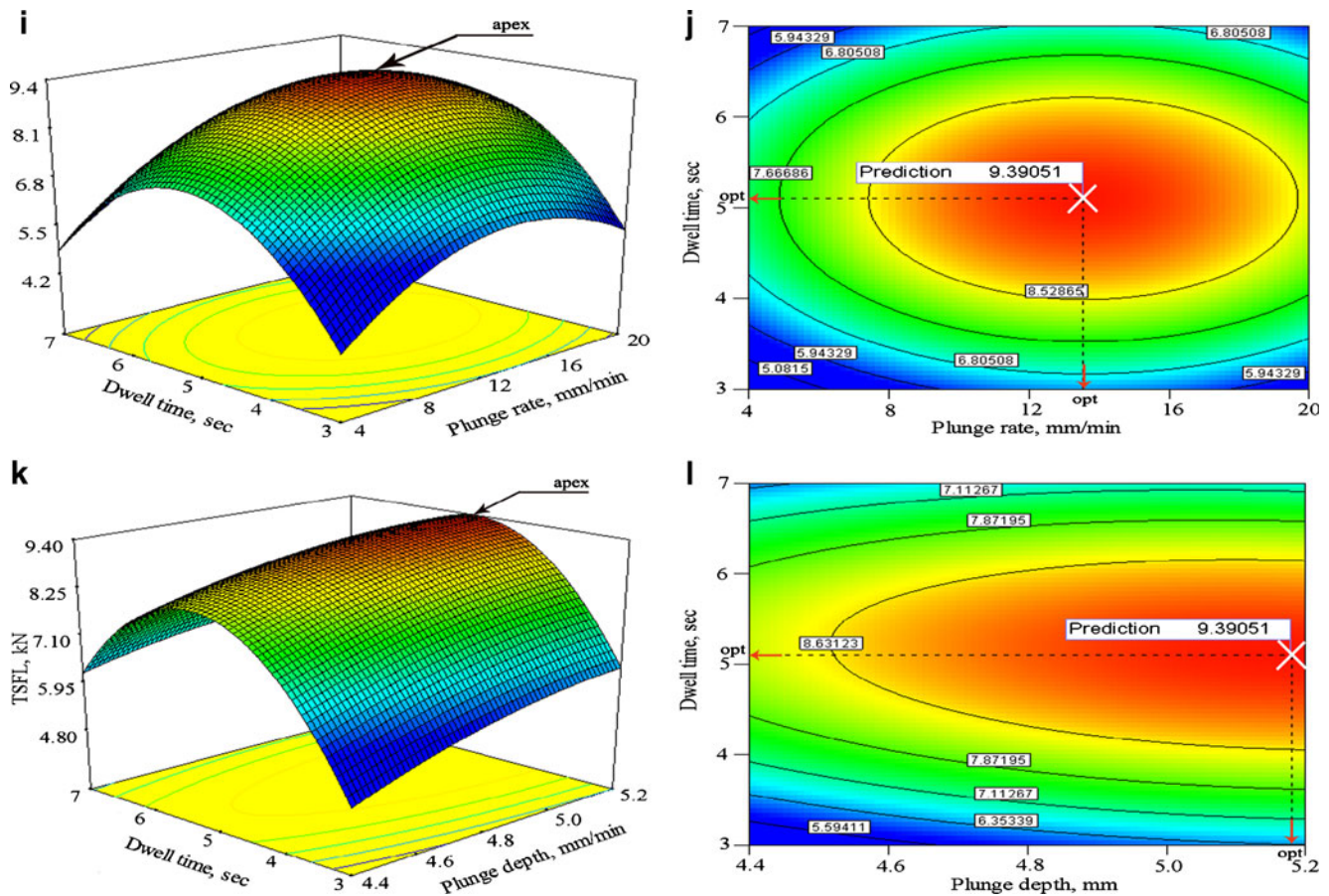


Fig. 4 (continued)

**Acknowledgements** The authors are grateful to the Department of Manufacturing Engineering, Annamalai University, for extending the facilities of Material Testing Laboratory to carry out this investigation. The authors also wish to record their sincere thanks to the Extramural Research & Intellectual Property Rights (ER&IPR), DRDO, New Delhi, for the financial support to carry out this investigation through a R&D project no. ERIP/ER/0703652/ M/01/1048.

## References

- Armao FG, Long RS, Winter EFM (1992) Joining techniques for aluminum castings, extrusions and sheet. Fugen von Aluminium-Entwicklung und Chancen, seminar Neu-Ulm
- Iwashita T (2003) Method and apparatus for joining. US Patent 6,601,751 B2
- Sakano R, Murakami K, Yamashita K, Hyoe T, Fujimoto M, Inuzuka M, Nagao U, Kashiki H (2001) Development of spot FSW robot system for automobile body members. In: Proceedings of the third international symposium of friction stir welding, Kobe, Japan, 27–28 Sep
- Sakaguchi S (1979) Resistant spot welding of aluminum alloy. J Light Metal Weld Construct 17(3):126–134, in Japanese
- Wang D, Liu S, Cao Z (2004) Study of friction stir welding of aluminum. J Mater Sci 39:1689–1693
- Pan T-Y, Joaquin A, Wilkosz DE, Reatherford L, Nicholson JM, Feng Z, Santella ML (2004) Spot friction welding for sheet aluminum joining. In: 5th international symposium on friction stir welding, The Welding Institute, Metz, France, paper no. 11A-1
- Arul SG, Pan T, Lin P-C, Pan J, Feng Z, Santella ML (2005) In: SAE Special Publication SP-1959, SAE International, Warrendale, PA, paper 2005-01-1256
- Mitlin D, Radmilovic V, Pan T, Chen J, Feng Z, Santella ML (2006) Structure-properties relations in spot friction welded (also known as friction stir spot welded) 6111 aluminum. Mater Sci Eng A 441:79–96
- Tozaki Y, Uematsu Y, Tokaji K (2007) Effect of tool geometry on microstructure and static strength in friction stir spot welded aluminum alloys. J Mach Tools Manuf 47:2230–2236
- Wang D-A, Chen C-H (2008) Fatigue lives of friction stir spot welds in aluminum 6061-T6 sheets. J Mater Process Technol 209 (1):367–375
- Badarinarayanan H, Yang Q, Zhu S (2009) Effect of tool geometry on static strength of friction stir spot-welded aluminum alloy. Int J Mach Tool Manufact 49:142–148
- Box GEP, Hunter WH, Hunter JS (1978) Statistics for experiment. Wiley, New York
- Khuri AI, Cornell J (1996) Response surfaces; design and analysis. Marcel Dekker, New York

14. Gunaraj V, Murugan N (1999) Application of response surface methodology for predicting weld bead quality in submerged arc welding of pipes. *J Mater Process Technol* 88:266–275
15. Tien CL, Lin SW (2006) Optimization of process parameters of titanium dioxide films by response surfaces methodology. *Opt Commun* 266:574–581
16. Phillip JR (1988) Taguchi techniques for quality engineering. Mc Graw-Hill, New York
17. Lakshiminarayanan AK, Balasubramanian V (2009) Comparison of RSM with ANN in predicting tensile strength of friction stir welded AA7039 aluminum alloy joints. *J Trans Nonferrous Met Soc China* 19:9–18